

1 **Title:** Selective deletion of glutamine synthetase in the mouse cerebral cortex induces glial  
2 dysfunction and vascular impairment that precede epilepsy and neurodegeneration

3

4 **Abbreviated title:** Cortical deletion of glutamine synthetase

5

6 **Authors:** Yun Zhou<sup>1\*</sup>; Roni Dhafer<sup>2</sup>; Maxime Parent<sup>3</sup>; Qiu-Xiang Hu<sup>1</sup>; Bjørnar Hassel<sup>4</sup>;  
7 Yee Siu-Pok<sup>5</sup>; Fahmeed Hyder<sup>3</sup>; Shaun E Gruenbaum<sup>2</sup>, Tore Eid<sup>1 2\*</sup>; Niels Christian  
8 Danbolt<sup>1\*</sup>

9

10 **Affiliations of all authors:** 1. Neurotransporter Group, Department of Molecular Medicine,  
11 Institute of Basic Medical Sciences, University of Oslo, N-0317 Oslo, Norway; 2.  
12 Department of Laboratory Medicine, Yale School of Medicine, New Haven, CT 06520,  
13 USA; 3. Magnetic Resonance Research Center, Yale School of Medicine, New Haven, CT  
14 06520, USA; 4. Department of Complex Neurology and Neurohabilitation, Oslo University  
15 Hospital, University of Oslo, N-0450 Oslo, Norway; 5. Department of Cell Biology,  
16 University of Connecticut Health, Farmington, CT 06030, USA.

17

18 **\*To whom correspondence should be addressed:** Yun Zhou (e-mail:  
19 [yun.zhou@medisin.uio.no](mailto:yun.zhou@medisin.uio.no)), Tore Eid (e-mail: [tore.eid@yale.edu](mailto:tore.eid@yale.edu)) or Niels Chr. Danbolt (e-  
20 mail: [n.c.danbolt@medisin.uio.no](mailto:n.c.danbolt@medisin.uio.no); web: [neurotransporter.org](http://neurotransporter.org)).

21

22 **Number: 7 Figures, 1 Table, 0 Multimedia, 0 3D models**

23 **Number of words:**

24 - Abstract: 188

25 - Introduction: 419

26 - Discussion: 1026

27

28 **Key words:** cerebrovascular dysfunction; epilepsy; Glul; neurodegeneration; metabolism;  
29 gliopathy

30

31 **Abbreviations:** CAS, Chemical Abstracts Service Registry Number; CVR,  
32 cerebrovascular reactivity; Glul, glutamate-ammonia ligase (a.k.a. glutamine synthetase,  
33 GS); cKO, conditional knockout; Cre, Cyclization recombinase; EAATs, excitatory amino  
34 acid transporters; EEG, electroencephalogram; EAAC1, excitatory amino acid carrier  
35 (EAAT3; slc1a1); GLAST, glutamate aspartate transporter (EAAT1; slc1a3); EAAT2,  
36 glutamate transporter 2 (EAAT2; slc1a2); GFAP, glial fibrillary acidic protein; fMRI,  
37 functional MRI; MRI, magnetic resonance imaging; MTLE, mesial temporal lobe epilepsy;  
38 NaPi, sodium phosphate buffer at pH 7.4; NCS, newborn calf serum; SDS, sodium dodecyl  
39 sulfate; WT, wild-type in the sense that the Glul gene is intact.

40

41

42 **Abstract**

43 Glutamate-ammonia ligase (glutamine synthetase; Glul) is enriched in astrocytes and  
44 serves as the primary enzyme for ammonia detoxification and glutamate inactivation in the  
45 brain. Loss of astroglial Glul is reported in hippocampi of epileptic patients, but the  
46 mechanism by which Glul deficiency might cause disease remains elusive. Here we  
47 created a novel mouse model by selectively deleting Glul in the hippocampus and  
48 neocortex. The Glul deficient mice were born without any apparent malformations and  
49 behaved unremarkably until postnatal week three. There were reductions in tissue levels  
50 of aspartate, glutamate, glutamine and GABA and in mRNA encoding glutamate receptor  
51 subunits GRIA1 and GRIN2A as well as in the glutamate transporter proteins EAAT1 and  
52 EAAT2. Adult Glul-deficient mice developed progressive neurodegeneration and  
53 spontaneous seizures which increased in frequency with age. Importantly, progressive  
54 astrogliosis occurred before neurodegeneration and was first noted in astrocytes along  
55 cerebral blood vessels. The responses to CO<sub>2</sub>-provocation were attenuated at four weeks  
56 of age and dilated microvessels were observed histologically in sclerotic areas of cKO.  
57 Thus, the abnormal glutamate metabolism observed in this model appeared to cause  
58 epilepsy by first inducing gliopathy and disrupting the neurovascular coupling.

59

60 **Highlights:**

- 61 # Most mice lacking cortical Glul survive despite abnormal glutamate signaling
- 62 # Lack of cortical Glul causes late-onset epilepsy and progressive neurodegeneration
- 63 # Progressive astrogliosis and vascular abnormalities preceded neurodegeneration

64

## 65 **1. Introduction**

66           Glutamate-ammonia ligase (glutamine synthetase; Glul) is enriched in astrocytes  
67 (Martinez-Hernandez *et al.*, 1977) and plays a critical role in the conversion of glutamate to  
68 glutamine and thereby also in the removal of neurotoxic ammonia in the central nervous  
69 system (CNS). Because treatment of rodents with the Glul inhibitor methionine sulfoximine  
70 induces convulsive seizures (Eid *et al.*, 2016) and because Glul is deficient in parts of the  
71 hippocampus in patients with mesial temporal lobe epilepsy (MTLE) (Eid *et al.*, 2004; van  
72 der Hel *et al.*, 2005), a role for Glul in epileptogenesis has been proposed. Consistent with  
73 this idea, the few described patients suffering from congenital Glul deficiency, all had  
74 neonatal onset, severe epileptic encephalopathy (Haberle *et al.*, 2012; Spodenkiewicz *et*  
75 *al.*, 2016).

76           The exact role of Glul in epilepsy, however, has been difficult to establish, and the  
77 mechanism by which Glul deficiency might cause disease is poorly understood. First,  
78 MTLE patients with secondary Glul deficiency may suffer from the consequences of the  
79 Glul deficiency as well as from effects of the primary insult (which is unknown in most  
80 cases). Second, the patients with congenital (primary) Glul deficiency were not only  
81 suffering from the cerebral consequences of Glul insufficiency, but also from the  
82 consequences of multiple organ failure with secondary effects on the brain (Spodenkiewicz  
83 *et al.*, 2016). Third, methionine sulfoximine has several effects other than inhibiting Glul. It  
84 decreases tissue glutathione (Shaw and Bains, 2002), increases astrocyte glycogen  
85 (Bernard-Helary *et al.*, 2002) and excites neurons via a Glul-independent mechanism  
86 (Kam and Nicoll, 2007). To separate the consequences of a primary Glul defect in the  
87 CNS from those of other events, a genetic approach is urgently needed; however,  
88 attempts to resolve this issue have been met with limited success. Mice completely  
89 deficient in Glul die already at embryonic day E3 (He *et al.*, 2007) and mice with deficiency  
90 limited to the CNS die three days after birth (He *et al.*, 2010).

91           Because cortical structures are important for seizure generation and propagation  
92 (Eid *et al.*, 2008; Blumenfeld *et al.*, 2009) and because intact brain stem functions are  
93 required for survival, we selectively deleted Glul in the cerebral cortex (i.e. neocortex and  
94 hippocampus) of mice by taking advantage of the Emx1-IRES Cre line, which directs Cre-  
95 mediated gene deletion in the cortex while sparing critical brain stem regions (Gorski *et al.*,  
96 2002). Using this approach, we demonstrate here that loss of cortical Glul causes  
97 abnormal glutamate signaling and induces astrogliosis and vascular impairment, ultimately  
98 culminating in spontaneous recurrent (epileptic) seizures and neuron loss.

## 99 **2. Materials and methods**

### 100 *2.1. Materials*

101 N,N' methylene bisacrylamide was from Promega (Madison, WI, USA). Molecular  
102 mass markers for SDS polyacrylamide gel electrophoresis (SDS PAGE) and nitrocellulose  
103 sheets (0.22  $\mu\text{m}$  pores, 100 % nitrocellulose) were from GE Healthcare (Buckinghamshire,  
104 UK). Paraformaldehyde was from Electron Microscopy Sciences (Hatfield, PA, USA), and  
105 glutaraldehyde was from TAAB (Reading, UK). Sodium dodecyl sulfate (SDS) of high  
106 purity (>99 % C12 alkyl sulfate) was from Millipore (Carrigtwohill, C. Cork, Ireland).  
107 Electrophoresis equipment was from Hoefer Scientific Instruments (San Francisco, CA,  
108 USA). Permout mounting medium, ProLong anti-fade DAPI media, DyNAzyme II DNA  
109 Polymerase were from ThermoFisher Scientific (Waltham, Massachusetts, USA). All other  
110 reagents were obtained from Sigma-Aldrich (St. Louis, MO, USA).

111

### 112 *2.2. Animals*

113 All animal studies were carried out in accordance with the European Communities  
114 Council Directive of 24 November 1986 (86/609/EEC) and the United States Animal  
115 Welfare Act. Formal approval to conduct the experiments was obtained from the animal  
116 subjects review board of the Norwegian Governmental Institute of Public Health (Oslo,  
117 Norway) and the Institutional Animal Care and Use Committee at the Yale School of  
118 Medicine. Care was taken to avoid suffering and minimize the number of the experimental  
119 animals. The mice were housed in individually ventilated (IVC) cages at constant  
120 temperature ( $22 \pm 0.7^\circ\text{C}$ ) and humidity ( $56 \pm 6\%$ ), and were fed with Harlan Teklad 2018  
121 (Harlan Laboratories Inc., Indianapolis, IN, USA) with the access to water *ad libitum*.  
122 Biopsies from ear or tail were collected for determining genotype.

123 As Figure 1A shows, to generate the conditional Glul KO mouse line (Glul<sup>fl/fl</sup>), the  
124 targeting vector was prepared by recombineering as described by Lee and co-workers

125 (Lee *et al.*, 2001). Briefly, approximately 12 kb of Glul genomic fragment containing the  
126 entire Glul was retrieved from the bacterial artificial chromosome (BAC) clone, RP24-  
127 326N10 (obtained from the BACPAC Resources Center at the Children's Hospital Oakland  
128 Research Institute, Oakland, CA) by gap repair. The 5'LoxP site as inserted in intron 1 at  
129 position 628, nucleotides 5' of exon 2, and the second 3'Lox sequence together with the  
130 Frt-PGKneo-Frt selectable marker was inserted 140 nucleotides 5' of exon 7. Thus, loxP  
131 sites were inserted on each flank of the DNA encoding exon 2-6. This vector containing  
132 approximately 4kb and 2.9kb of 5'-long and 3'-short arms, respectively, was then  
133 linearized by NotI digestion, purified and then electroporated into ES cells, which was  
134 derived from F1(129sv/C57BL6j) blastocyst. ES cells were cultured in the presence of  
135 G418 and Ganciclovir after electroporation according to Wurst and Joyner (Wurst and  
136 Joyner, 1999) and drug resistant colonies were picked and cultured in 96-well plates. Drug  
137 resistant ES clones were screened by nested long-range PCR using primers specific to  
138 genomic sequences outside the homology arms and LoxP sites to identify targeted ES  
139 clones. Targeted clones were expanded and screened again to confirm their identity prior  
140 to the generation of chimeric animals by aggregation with CD1 morula. Chimeric males  
141 were then bred with ROSA26-Flpe female (Soriano, 1997) to remove the PGKneo cassette  
142 to generate the final Glul floxed allele. Two chimeric founder lines (1F7 and 1B4) were  
143 produced, and backcrossed more than ten generations into the C57BL/6 background. Both  
144 were crossed with Cre-lines as described. The Flox-Glul mice were first tested by crossing  
145 with a general deleter strain (Htrp1-Cre: Jackson Laboratories, Stock No. 004302; RRID:  
146 IMSR\_JAX:004302) mediating deletion in all cells including germ cells and a global  
147 astrocyte deleter (hGFAP-Cre: Jackson Laboratories, Stock No. 004600; RRID:  
148 IMSR\_JAX:004600). Heterozygote Glul mice of two lines were obtained and they were  
149 fertile, but homozygote knockout mice were not obtained (data not shown) in agreement  
150 with data from others using another Flox-Glul mouse line (He *et al.*, 2007; He *et al.*, 2010).

151 We then tested the Emx1-IRES-Cre line (Jackson Laboratories, Stock No. 005628; Gorski  
152 *et al.*, 2002; RRID: IMSR\_JAX:005628)) by crossing it with a reporter line  
153 [Gt(ROSA)26Sor<sup>tm4</sup>(ACTB-tdTomato,-EGFP)<sup>Lu0</sup>; Jackson Laboratories, Stock No. 007676; RRID:  
154 IMSR\_JAX: 007676). The resultant litters had Cre expressed in neurons, astrocytes and  
155 oligodendrocytes, (data not shown) consistent with data from others (Gorski *et al.*, 2002).  
156 Crossing the female or male Emx1-IRES-Cre line with the male or female Flox-Glul mice  
157 resulted in live mice lacking Glul in the cerebral cortex (Fig. 1B). The breeding scheme to  
158 generate cortical Glul knockouts was as follows:

159         1<sup>st</sup> generation: heterozygote Cre-mice ([Emx1-Cre<sup>+0</sup>]) were crossed with  
160 homozygote Flox-Glul mice ([Glul<sup>f/f</sup>]). This crossing gave two possible genotype  
161 combinations, namely [Emx1-Cre<sup>+0</sup>;Glul<sup>f/w</sup>] and [Glul<sup>f/w</sup>].

162         2<sup>nd</sup> generation: the [Emx1-Cre<sup>+0</sup>;Glul<sup>f/w</sup>] mice were crossed with homozygote Flox-  
163 Glul mice ([Glul<sup>f/f</sup>]). This crossing gave four possible genotype combinations: [Emx1-  
164 Cre<sup>+0</sup>;Glul<sup>f/f</sup>], [Emx1-Cre<sup>+0</sup>;Glul<sup>f/w</sup>], [Glul<sup>f/f</sup>] and [Glul<sup>f/w</sup>].

165

166 The [Emx1-Cre<sup>+0</sup>;Glul<sup>f/f</sup>] mice are hereafter referred to as cortical knockouts (cKO), while  
167 the [Emx1-Cre<sup>+0</sup>;Glul<sup>f/w</sup>] are referred to as conditional heterozygotes and the mice lacking  
168 Cre ([Glul<sup>f/f</sup>] and [Glul<sup>f/w</sup>]) are referred to as wildtype (WT).

169         The phenotypes of the two Flox-Glul founder lines were similar (data not shown).

170 Most of our study here was based on the knockout generated from the 1F7 founder line.

171

### 172 2.3. Genotyping

173         Biopsies were digested (95°C, 1 h) with alkaline lysis solution (25 mM NaOH and  
174 0.2 mM EDTA) and chilled on ice before addition of neutralizing solution (40 mM Tris-HCl).  
175 The primers to detect the GS-flox genotype were GS lox gtF (5'-agtcagcagtgctccttg-3')  
176 and GS lox gtR (5'-gctcagctcttgaacaacc-3'). The cycle is described as following: 1. 94°C 3



177 min; 2. 94°C 30 sec; 3. 55°C 30 sec; 4. 72°C 30 sec; Repeat 2-4 for 35 cycles; 5. 72°C, 4  
178 min. The expected PCR products were 346 bp for the wild-type allele and 440 bp for the  
179 flox allele. The primers to detect the Emx1-Cre (Gorski *et al.*, 2002) are oIMR1084 (5'-  
180 GCG GTC TGG CAG TAA AAA CTA TC-3') and oIMR1085 (5'-GTG AAA CAG CAT TGC  
181 TGT CAC TT-3'). The cycle is described as following: 1. 94°C 3 min; 2. 94°C 30 sec; 3.  
182 51.7°C 1 min; 4. 72°C 1 min; steps 2-4 were repeated 35 times; 5. 72°C, 2 min. The  
183 expected PCR product was about 100 bp (data not shown).

184

#### 185 2.4. Antibodies

186 Affinity purified anti-peptide antibodies to sheep anti-EAAT2 (GLT-1; Ab#8; Li *et al.*,  
187 2012; RRID: AB\_2714090), rabbit anti-EAAT1 (GLAST; Ab#314; Holmseth *et al.*, 2009;  
188 RRID: AB\_2314561) and rabbit anti-EAAT3 (EAAC1; Ab#371 Holmseth *et al.*, 2012a;  
189 RRID: AB\_2714048) were from the same batch as previously described. Because  
190 antibody batches may differ from each other (Danbolt *et al.*, 2016a), we identify antibody  
191 batches by the unique identification number ("Ab#") they are given by our electronic  
192 laboratory information system (software provided by Science Linker AS; Oslo, Norway).

193 Rabbit anti-VGLUT1 (Cat. No. 135303; RRID: AB\_887875) was gifts from Henrik  
194 Martens (Synaptic System GmbH, Goettingen, Germany). Rabbit anti-GLUT1 (Cat. no.  
195 ab14683; RRID: AB\_301408) were from Abcam. Rabbit anti-glutamine synthetase (Cat. no  
196 G2781; RRID: AB\_259853), and mouse monoclonal anti-GFAP (Cat no. G3893; RRID:  
197 AB\_477010) were from Sigma (St. Louis, MO, USA). IRDye 680RD Donkey anti-Rabbit  
198 IgG (H+L) (Cat. no. P/N 926-68073; RRID: AB\_10954442) and IRDye 800CW Donkey  
199 anti-mouse IgG (H+L) (Cat. no. P/N 926-32212; RRID: AB\_621847) were from Li-Cor  
200 Bioscience UK Ltd, and Alexa Fluor 680 AffiniPure Donkey anti-sheep IgG (H+L) (Cat. no.  
201 713-625-147; RRID: AB\_2340753) was from Jackson ImmunoResearch. Alexa fluor goat  
202 anti-mouse 488 (Cat. no A11029; RRID: AB\_2534088), goat anti-rat 488 (Cat. no A11006;

203 RRID: AB\_2534074), goat anti-rabbit 555 (Cat. no A21429; RRID: AB\_2535850)

204 antibodies were purchased from Molecular probes (Eugene, OR, USA).

205

## 206 2.5. Tissue preparation for electrophoresis and immunoblotting

207 The tissue wet weight was recorded before the tissue was homogenized in 10-20  
208 volumes of 1% SDS in 10 mM sodium phosphate buffer (NaPi) with pH 7.4 (NaPi). As  
209 brain tissue contains close to 10 % protein (Lowry, 1953; Lowry *et al.*, 1954), the wet  
210 weight gave a first approximation of the protein content. The total protein concentrations of  
211 the extracts were subsequently determined by Lowry assay (Lowry *et al.*, 1951), and then  
212 diluted to the same concentrations in SDS-sample buffer (Laemmli, 1970), and loaded  
213 onto SDS-polyacrylamide gel (Laemmli, 1970) using Hamilton syringes (Hamilton Robotics,  
214 NV, USA) to ensure correct loading. After electrophoresis and immunoblotting, Ponceau-S  
215 stain or total REVERT protein staining (Li-Cor, Lincoln, NE, USA) of the membranes in  
216 combination with Coomassie blue stain of the gels were used to check that the blots  
217 indeed had received equal amounts of protein after transfer. Identical blots were prepared  
218 in parallel and probed with different primary antibodies. Because the expression of  
219 housekeeping proteins can alter in diseased state (Ferguson *et al.*, 2005) and glutamine  
220 synthetase deficiency in murine cortex causes progressive neurodegeneration, house  
221 keeping proteins might not be optimal as useful references in the present study, and were  
222 only used when stated.

223 Briefly, the blots were first rinsed in PBS (10 mM NaPi pH7.4 and 135 mM NaCl)  
224 and then were blocked (1 hour) with 0.05 % (w/v) casein in PBS before incubating with  
225 primary antibodies in bovine serum albumin (BSA; 30 mg/ml) in PBST (PBS with 1 ml/liter  
226 Tween 20 and 0.5 mg/ml NaN<sub>3</sub>) overnight, room temperature. The membrane was rinsed  
227 (4x10 min) with PBST before incubation (1 hour) in secondary antibody solution (1:20000).  
228 Rinse membrane several times with PBST and then PBS to remove residual Tween 20

229 before scanning. The blots were examined for immunofluorescence using an infrared  
230 scanner (Licor Odyssey system, LI-COR Biotechnology-UK Ltd, Cambridge, UK).  
231 Densitometric data were extracted from the images using the Gel analyzer tool included in  
232 our electronic laboratory information system (software provided by Science Linker AS;  
233 Oslo, Norway). The results are presented as percent of control (average  $\pm$  SEM where n  
234 represents the number of pairs of littermates). Unpaired student's T-test was used to  
235 compare the means of two groups of data. P-values are given when there were statistically  
236 significant differences ( $p < 0.05$ ) between the data from the Emx1-Glul knockout mice and  
237 the control mice.

238

## 239 2.6. Immunocytochemistry

240 Mice were transcardinally perfused with 4% formaldehyde in 0.1M NaPi with or  
241 without 0.05% glutaraldehyde (Danbolt *et al.*, 1998). Briefly, they were deeply  
242 anesthetized by intraperitoneal injection with ZFR cocktail (at least 0.1 ml per 10 g body  
243 weight). ZRF is of a mixture of zolazepam (3.3 mg/ml; CAS 31352-82-6), tiletamine (3.3  
244 mg/ml; CAS 14176-49-9), xylazine (0.5 mg/ml; CAS 7361-61-7) and Fentanyl (2.6  $\mu$ g/ml;  
245 CAS 437-38-7). After cessation of all reflexes, the mice were perfused first with 0.1 M NaPi  
246 pH7.4 to wash out blood and then immediately followed by 4 % formaldehyde in 0.1 M  
247 NaPi with or without 0.05 % glutaraldehyde, as stated, for five minutes. The relevant  
248 tissues were collected and immersed in fixative for about 2-4 hour at room temperature.  
249 Sections (40  $\mu$ m thick) were cut from the fixed unfrozen tissue using a Vibratome 1000  
250 plus® (Vibratome, Bannockburn, UK).

251 Diaminobenzidine-peroxidase labeling was performed as described (Lehre *et al.*,  
252 1995). Briefly, the sections were pre-incubated in 1 % hydrogen peroxide in 0.1 M NaPi,  
253 rinsed and treated (30 min, room temperature) in 1 M ethanolamine in 0.1 M NaPi with  
254 0.5 % (v/v) Triton X-100 and rinsed (x 3) in PBS (0.135 M NaCl, 10 mM NaPi pH 7.4 with

255 0.5 % (v/v) Triton X-100) prior to incubation (1 h, room temperature) in blocking solution  
256 (10 % (v/v) newborn calf serum (NCS) in TBST (TBS with 0.5 % (v/v) Triton X-100), with  
257 0.1 mg/mL NaN<sub>3</sub>). Next, sections were incubated (over night, room temperature) with  
258 primary antibodies diluted (at concentrations as stated) in blocking solution. After rinsing (x  
259 5) in TBST with 1 % (v/v) NCS, the sections were incubated (1 h, room temperature) with  
260 secondary antibodies diluted (1:300) in TBST with 1 % (v/v) NCS, and, after rinsed as  
261 above, incubated (1 h, room temperature) with streptavidin-biotinylated horseradish  
262 peroxidase complex, diluted (1:300) in TBST with 1 % (v/v) NCS. The rinsing steps were  
263 repeated and sections were then rinsed (x3) in PBS prior to the color development step  
264 with diaminobenzidine-peroxidase.

265 Immunofluorescent labeling was done as previously described (Zhou *et al.*, 2012).  
266 Briefly, The sections were rinsed (3 x 5 min) in TBST (TBS with 0.5 % Triton X-100),  
267 treated with 1 M ethanolamine in 0.1 M NaPi pH 7.4 for 30 min, washed in TBST,  
268 incubated (1 hour) in TBST containing 10 % newborn calf serum and 3 % bovine serum  
269 albumin followed by incubation with primary antibodies and finally with secondary  
270 antibodies (Alexa fluor goat anti-mouse 488, Molecular probes; Eugene, OR, USA) diluted  
271 1:1000 dilution. After being washed 3 times with TBST, the sections were then mounted  
272 with ProLong Gold antiFade mounting medium with DAPI (ThermoFisher Cat. No. P36935,  
273 Waltham, MA, USA) or Fluoroshield with DAPI histology mounting medium (Sigma, F6057)  
274 and examined using a Zeiss Axioplan 2 microscope equipped with a Zeiss LSM 510 meta  
275 confocal scanner head (Zeiss, Jena, Germany).

276

## 277 *2.7. Histological staining*

### 278 *2.7.1. Nissl staining*

279 Sections were mounted onto SuperFrost Plus slides (ThermoFisher, Waltham, MA,  
280 USA), air dried and incubated (3 min) in Walter's cresyl violet solution on a heating plate.

281 Excess staining solution was removed, the stain was differentiated in tap water (3 min) and  
282 the sections were dehydrated in graded ethanol, cleared in xylene and mounted with  
283 Permount (Cat. no: 12377369, Fisher Scientific).

284

### 285 *2.7.2. NeuroSilver staining*

286 Vibratome sections were stained using the FD NeuroSilver kit according to the  
287 manufacturer's instructions (FD NeuroTechnologies Inc, Columbia, USA). Briefly,  
288 sections were rinsed in MilliQ water (2 x 5 min), transferred into a mixture containing equal  
289 volumes of Solution A and B (2 x 10 min) and incubated in a mixture of equal volumes of  
290 Solution A and B with Solution E, and then in a mixture of Solution C and Solution F (2 x 2  
291 min). After incubation in a mixture of Solution D and Solution F for 5 min, the sections were  
292 rinsed in MilliQ water (2 x 3 min) and incubated in Solution G (2 x 5 min). The sections  
293 were finally mounted on SuperFrost slides, air dried, cleared in xylene and coverslipped  
294 with Permount.

295

### 296 *2.8. Amino acid measurements*

297 Mice were decapitated, and the heads immediately plunged into liquid nitrogen for 5  
298 second. The neocortex and hippocampi were dissected out on ice, weighed, and  
299 homogenized in 10 volumes of perchloric acid, 2% (vol/vol) containing  $\alpha$ -amino adipate, 1  
300 mmol/L. Protein was removed by centrifugation, and the supernatant was neutralized with  
301 KOH, 10 mol/L. Amino acids were quantified by HPLC and fluorescence detection after  
302 pre-column derivatization with o-phthaldialdehyde, as described (Dahlberg *et al.*, 2014).

303

### 304 *2.9. EEG*

305 Mice were anesthetized with 0.25-2% isoflurane (Baxter, Deerfield, Ill.) in O<sub>2</sub>,  
306 placed in a stereotaxic frame (David Kopf Instruments, Tujunga, CA, USA) and implanted

307 with stainless-steel screw electrodes (Plastics One, Roanoke, Va, USA) that were  
308 positioned in the epidural space, over the parietal cortex bilaterally. The female ends of the  
309 electrodes were inserted in a pedestal (Plastics One, Roanoke, VA; USA) which was  
310 cemented onto the skull with UV light cured acrylated urethane adhesive (Loctite 3106  
311 Light Cure Adhesive, Henkel Corp., Rocky Hill, CT, USA) to form a headcap. The mice  
312 were placed individually in custom-made Plexiglas cages. A 6-channel cable was  
313 connected to the electrode pedestal on one end and to a commutator (Plastics One) on  
314 the other. A second cable connected the commutator to the digital EEG recording unit  
315 (CEEGraph Vision LTM, Natus/Bio-Logic Systems Corp., San Carlos, CA, USA). Digital  
316 cameras with infrared light detection capability were used to record animal behavior (two  
317 cages per camera). The digital video signal was encoded and synchronized to the digital  
318 EEG signals. Seizures were identified by visual inspection of the EEG record. The Racine  
319 criteria (Racine *et al.*, 1973) were modified and used to classify the seizures from the video  
320 records, as follows: Stage 1, immobilization, eye blinking, twitching of vibrissae, and mouth  
321 movements; Stage 2, head nodding, often accompanied by severe facial clonus; Stage 3,  
322 forelimb clonus; Stage 4, rearing, Stage 5, rearing, falling, and generalized convulsions.

323

#### 324 *2.10. fMRI imaging and data analysis*

325 For imaging experiments, animals were first anesthetized using 3% isoflurane in a  
326 mixture of O<sub>2</sub> and N<sub>2</sub>O (30/70%), then placed in a custom built frame where they were  
327 freely breathing through a nose cone. During the scanning procedure, isoflurane was  
328 turned off and anesthesia was maintained using a subcutaneous infusion of  
329 dexmedetomidine (Zoetis): 2μL + 4μL/h per gram of body weight, at 0.05 mg/mL  
330 concentration. Body temperature was monitored using a rectal probe, and maintained  
331 within 35-37°C using warm water pumped through the bed.

332 MRI data were obtained on a modified 9.4T system with Varian spectrometer and  
333 custom built 1H 12mm surface coil. Images were acquired over 8 contiguous coronal  
334 slices (thickness = 1mm), covering the parenchyma between the olfactory bulb and  
335 cerebellum, with an in-plane field of view of 1.28 x 1.28 cm. Resting-state (task-free)  
336 images were obtained using an echoplanar imaging (EPI) sequence (TR/TE= 1000/13 ms  
337 in a 32 x 32 matrix, for an in-plane resolution of 250 $\mu$ m) for 6 minutes (360 repetitions),  
338 and repeated three times per animal. The cerebrovascular reactivity (CVR; repeated twice  
339 per animal) functional scans lasted for 9 minutes with 10% CO<sub>2</sub> added to the breathing  
340 gas mixture between minutes 3 and 6 of the acquisition. Lastly, a high-resolution spin-echo  
341 anatomical image (32 slices at 0.25 mm thickness, 128 x 128 for an in-plane resolution of  
342 100 $\mu$ m, 4 averages) was used for co-registration and volumetric analysis.

343 . Using AFNI (<https://afni.nimh.nih.gov/>), functional images of CO<sub>2</sub> challenge were  
344 corrected for motion and spatially smoothed using a Gaussian filter (FWHM = 1 mm).  
345 Parametric maps of CVR were generated from a voxel-level linear model and expressed  
346 as the t-statistical value of the contrast between baseline (Frames 1 to 180) and CO<sub>2</sub>  
347 challenge (Frames 210 to 360).

348 Anatomical images were used to generate a non-linear transform from each animal  
349 subject's native space to a common standard space. The transform was then applied to  
350 all parametric maps of CVR, which were then Fisher transformed. Group averages and  
351 contrasts were calculated with a voxel-level linear model for each modality with an  
352 adjusted threshold of  $p < 0.05$  corrected for multiple comparisons. Finally, brain volume  
353 was estimated by manually drawing an intracranial mask over the anatomical images (in  
354 native space) by an experimenter blinded to group conditions.

355

356 *2.11. Open field test (OF)*

357 The 15-min OF tests were carried out using 4-15 weeks old (male and female) under a  
358 light intensity of  $100 \pm 10$  Lux. The tests were performed between 4.0-0.5 hours before the  
359 start of dark cycle. First, animals were placed in the testing room in their home cage for at  
360 least 10 min to acclimate. The test started by gently removing each mouse from their  
361 home cage and immediately placing them in the center of the test chamber (chamber  
362 dimensions: L50 x W50 x H21.5 cm). A series of 12.5 x 12.5 cm zones were defined in the  
363 test chamber. The outer zone consists of 12 blocks while the center/inner zone consists of  
364 4 blocks. The entire session was videotaped for later analysis. All the animals were first-  
365 time for OFs. After the tests, the animals were housed in a new cage, and the number of  
366 feces produced during the sessions was counted. 70 % ethanol was used to clean the  
367 chamber between sessions. All OF videos were then analyzed by one individual in a  
368 double-blind manner. Horizontal activities were measured by total number of crossings  
369 (during each min and in 15 min) and vertical activities were measured by the total number  
370 of rearing (to the walls). For accessing anxiety behavior, both total number of crossings to  
371 the center and the number of fecal boli produced were counted

372

### 373 *2.13. Experimental Design and statistical analysis*

374 All experiments were performed at least three times unless stated otherwise.  
375 Statistical significance between two independent samples was assessed by Student's t  
376 test. Statistical analyses and plotting graphs were performed with GraphPad Prism4  
377 (GraphPad Software). Differences between groups were judged to be significant when P  
378 values were smaller than 0.05. \*, \*\* and not significant represent  $P < 0.05$ ,  $P < 0.01$  and not  
379 significant, respectively. Error bars always indicate the standard error of the mean ( $\pm$  SEM)  
380 except when stated (Table 1). No samples or animals were excluded from the analysis.  
381 For HPLC analysis, data were obtained in a blind manner in which the experimenters did  
382 not know the mouse genotypes.



383

### 384 **3. Results**

#### 385 *3.1. Mice with cortical deletion of Glul are viable*

386 Our model of cortical Glul deficiency was created by first tagging the Glul gene with  
387 flanking LoxP sites to permit cyclization recombinase (Cre)-mediated deletion of exons 2-6  
388 (Fig. 1A). These animals are hereafter referred to as Glul-flox mice. We then crossed the  
389 Glul-flox mice with Emx1-IRES-Cre mice, in which Cre-expression is primarily restricted to  
390 telencephalic regions, in particular parts that give rise to the neocortex and hippocampus  
391 (Gorski *et al.*, 2002).

392 Breeding of our Glul-flox mice with the Emx1-Cre mice resulted in conditional  
393 knockout (cKO) mice where the Glul protein was abolished in most of the neocortex and  
394 hippocampus (Fig. 1BC). Because Glul is predominantly an astroglial enzyme, it seems  
395 reasonable to assume that the Emx1-Cre driven deletion mostly affects astrocyte function.

396 The glutamate transporters EAAT3 (Fig. 1C) and EAAT2 (data not shown) were still  
397 present in the affected area, as these genes had not been floxed and therefore could not  
398 be excised by Cre. The cortical expression levels of Glul protein in heterozygous mice  
399 were approximately half of those in wild-type (WT) mice (52%, n = 2 pairs of mice). Further,  
400 we observed that Glul protein was absent from the cKO cortex at birth (data not shown),  
401 consistent with the reported start of Cre-expression at E10.5 (Gorski *et al.*, 2002).

402 Genotyping at 3 weeks of age from a breeding scheme (Cre<sup>+/-</sup>; Glul<sup>f/w</sup> x Cre<sup>0/0</sup>; Glul<sup>f/f</sup>)  
403 revealed a typical Mendelian distribution (2WT: 1Het : 1cKO) of 47.8 % wild-type (WT;  
404 Cre<sup>0/0</sup>; Glul<sup>f/f</sup> or f/wt, n=199), ~27.2 % heterozygous (Cre<sup>+/-</sup>; Glul<sup>f/w</sup>, n=113) and ~25.0% cKO  
405 mice (Cre<sup>+/-</sup>; Glul<sup>f/f</sup>; n=104). Thus, the deletion did not appear to increase prenatal mortality.  
406 Increased mortality was first noted after three weeks (Fig 1D).

407

#### 408 *3.2. Cortical deletion of Glul results in late-onset epileptic seizures*

409 Despite deletion of *Glul* before birth, neither heterozygous nor homozygous cKO  
410 mice could be distinguished from their WT littermates with respect to overall appearance  
411 during the first two postnatal weeks. At postnatal week 3, the cKO mice began to exhibit  
412 behavioral abnormalities such as hypoactivity and periodic running fits when subjected to  
413 mild stimulation such as removing the cage lid or gentle knocking on the cage. To further  
414 assess the behavioral phenotype, we subjected the mice to the open field test which  
415 measures general locomotive activities. The mice (4-15 weeks old cKO and WT littermates)  
416 were observed for 15 min each. This was sufficient to reveal alterations in the locomotive  
417 activities (Fig. 2). One subgroup of the cKO mice (cKO1, 9 pairs of WT and cKO) were  
418 almost inactive during the test (Fig. 2AC) while another subset (cKO2, 6 pairs) showed  
419 hypoactivity interrupted by bursts of sudden wild running (Fig. 2BC). The cKO mice  
420 exhibited reduced vertical activity (Fig. 2D) and fewer entries to the center of the chamber  
421 (Fig. 2E), while the time spent in the center by the cKO mice was comparable to that of  
422 WT littermates (Fig. 2F). During these sessions, fewer fecal boli were produced by the  
423 cKO mice, suggestive of reduced anxiety (Fig. 2G).

424 Besides periodic running fits, facial automatisms with occasional falling and forelimb  
425 clonus were observed in the cKO mice older than 6 weeks, suggestive of seizures.  
426 Continuous video-intracranial EEG recordings of mice aged 4 – 28 weeks demonstrated  
427 spontaneous recurrent seizures in 4 of 7 cKO mice, but not in any of the heterozygous  
428 (n=9) or in the WT (n=11) mice (Fig. 3). The frequency, duration and behavioral severity of  
429 the seizures varied among animals, with a tendency for the seizures to become more  
430 frequent as the animals aged.

### 431 3.3. Cortical deletion of *Glul* causes progressive neurodegeneration and ultimately 432 hippocampal sclerosis

433 Examination of Nissl-stained brain sections from 6 weeks old *Glul* cKO mice did not  
434 reveal any major abnormalities in the neocortical and hippocampal cytoarchitecture.

435 However, focal lesions (small islands of neuronal loss) in the neocortex were occasionally  
436 found at this age, but only in some of the mice (data not shown). As the mice aged, more  
437 obvious neuropathological changes started in the hippocampus, as evidenced by selective  
438 degeneration of CA1 and CA3 pyramidal neurons and dentate granule cells. The  
439 hippocampal pathology occurred bilaterally and was readily apparent in the third postnatal  
440 month (Fig. 4AB). As the mice aged further, the neocortex became progressively affected  
441 in multiple areas, particularly the retrosplenial, motor, somatosensory, parietal association  
442 and visual cortices (Fig. 4C-E). The degree and pattern of neocortical neurodegeneration  
443 varied among animals at similar ages, but generally started in the most superficial layer of  
444 the cortex (data not shown). Neuro-Silver staining at 11 weeks of age (Fig. 4BD) confirmed  
445 that large numbers of neurons were degenerating in the cKO mice, but not in the  
446 conditional heterozygotes ( $Emx1-Cre^{+/0}; Glul^{f/w}$ ) and the WT (Cre negative) mice.

447

#### 448 *3.4. Astrocytes lacking Glul become reactive prior to neuronal loss and epilepsy*

449 Considering that Glul is an astrocytic protein, we assessed for reactive astrogliosis  
450 by examining the expression of glial fibrillary acid protein (GFAP). Western blotting  
451 revealed that the protein was hardly increased in cKO mice versus WT littermates at 2  
452 weeks of age (Fig. 5B), but showed significant increases at 4 weeks of age, consistent  
453 with progressive astrogliosis. The increase in GFAP was confirmed by Taqman RT-PCR  
454 (data not shown) and immunocytochemistry (Fig. 5A).

455

#### 456 *3.5. Loss of Glul impacts the molecular anatomy and physiology of cerebral blood vessels*

457 Interestingly, the expression of GFAP was increased in astroglial processes along  
458 blood vessels in the cKO mice as early as 3 weeks of age (Fig. 6AB). Further, at later  
459 stages, the vessels became markedly dilated in the areas of the neocortex and of the  
460 hippocampus where neurodegeneration was occurring. (Fig. 6C). We therefore asked

461 whether the astroglial reactivity was associated with changes in the physiology of cerebral  
462 blood vessels. MRI cerebrovascular reactivity (CVR), defined as the relative increase in  
463 Blood Oxygen Level Dependent (BOLD) signal during a CO<sub>2</sub> challenge, revealed  
464 significant differences between WT and cKO mice at 4 weeks and 12-15 weeks of age (Fig.  
465 6D). In both age groups, CVR was reduced in neocortical areas, such as cingulate and  
466 sensorimotor cortices in the cKO mice (4 weeks: WT, 5.44 ± 0.65%; cKO, 2.8 ± 0.58%; 12-  
467 15 weeks: WT, 5.65 ± 1.17%; cKO, 1.67 ± 0.44%). In the dorsal hippocampus, a reduction  
468 of CVR was noted at 4 weeks of age in the cKO mice, but not at 12-15 weeks of age (4  
469 weeks: WT, 4.37 ± 0.75%; cKO, 2.24 ± 0.35%; 12-15 weeks: WT, 3.35 ± 0.37%; cKO, 3.03  
470 ± 0.33%). In subcortical areas spared from Glul deletion like the basal forebrain, no  
471 significant group effect was found at either age (4 weeks: WT, 3.22 ± 0.59%; cKO, 2.81 ±  
472 0.41%; 12-15 weeks: WT, 2.39 ± 0.37%; cKO, 2.88 ± 0.46%).

473

### 474 3.6. Young mice lacking cortical Glul have abnormal glutamate signaling

475 As Glul is critical for the homeostasis of glutamate, glutamine and GABA, and as  
476 cerebral blood flow is regulated through glutamate-mediated astrocyte responses (Attwell  
477 *et al.*, 2010), we quantified the levels of these and other amino acids in the cKO and WT  
478 brains (Table 1). As expected, the concentrations of glutamine, glutamate, aspartate and  
479 GABA in the tissue were significantly lower in the cKO cortex than in the WT cortex,  
480 whereas no changes were observed in the cerebellum, which expressed normal levels of  
481 Glul (Fig. 1BC).

482 We also assessed several molecules involved in glutamate signaling by Taqman  
483 RT-PCR (Fig. 7A) and found reduced levels of mRNA encoding the major glial glutamate  
484 transporter EAAT2 and of mRNA encoding the glutamate receptor subunits GRIA1 (GluR1)  
485 and GRIN2A (GluN2A) in the hippocampi of 5 weeks old cKO mice. Immunoblotting of  
486 EAAT2 showed that the reduction in EAAT2 protein levels was present already at 2 weeks

487 of age (Fig. 7B). Another glial glutamate transporter, EAAT1, displayed a similar  
488 expression pattern albeit less pronounced, while the expression of EAAT3 (which is the  
489 major neuronal glutamate transporter at the plasma membrane: Holmseth *et al.*, 2012b)  
490 and neuronal vesicular glutamate transporter VGLUT1 were not changed significantly.

491

#### 492 **4. Discussion**

493 The exact role of Glul in the etiology of CNS disease, including epilepsy, is poorly  
494 understood due to the lack of viable and specific *in vivo* approaches. To overcome this  
495 hurdle, we selectively deleted Glul in the cerebral cortex of mice. This resulted in a viable  
496 Glul knockout model and proved that a selective loss of cortical Glul is, by itself, sufficient  
497 to cause epileptic seizures and progressive neurodegeneration resembling hippocampal  
498 sclerosis. The mutation had a high penetrance considering that the C57BL6 mouse strain  
499 used here is relatively resistant to epileptic seizures (McLin and Steward, 2006).

500 However, the first behavioral seizures or neurodegeneration were only evident in  
501 animals six weeks of age or older, even though changes in brain chemistry, glial cells and  
502 cortical blood vessels had been present for several weeks. Thus, seizures and  
503 neurodegeneration are likely not directly caused by the Glul deficiency, but rather occur as  
504 a consequence of a pathological process involving reactive astrocytes and impaired  
505 neurovascular coupling. These slowly developing effects of Glul deficiency are distinctly  
506 different from the rapid, excitotoxic syndrome with early seizures and increased mortality  
507 seen in EAAT2 knockout mice (Tanaka *et al.*, 1997; Zhou *et al.*, 2014).

508 It is well known that brain tissues from humans with epilepsy and from animal  
509 models of the disease contain reactive astrocytes and altered blood vessels (Eyo *et al.*,  
510 2017; Wolf *et al.*, 2017). While these changes were originally regarded as secondary  
511 responses to injury, more recent studies have shown that reactive astrocytes can induce  
512 neuronal hyperexcitability and spontaneous seizures irrespective of the primary initiating

513 event (Ortinski *et al.*, 2010; Robel *et al.*, 2015). In line with this gliopathy hypothesis of  
514 epilepsy (Verkhratsky *et al.*, 2012; Coulter and Eid, 2012; Robel and Sontheimer, 2016),  
515 we observed reactive astrocytes weeks before the first seizure and neuron loss were  
516 detected.

517           Further, astrocytes, particularly their cytoplasmic processes, are integral  
518 elements of the neurovascular unit and can control vessel diameter (Attwell *et al.*, 2010).  
519 Numerous changes in the molecular anatomy of microvessels in Glul-deficient brain  
520 regions in patients with TLE and animal models of the disorder have been demonstrated  
521 (Eid *et al.*, 2016). However, whether these changes are a cause or consequence of  
522 seizures has remained unclear. Here we show, for the first time, that deletion of astrocytic  
523 Glul leads to increased vascular caliber and lack of vasodilation in response to CO<sub>2</sub>.  
524 These changes were present *before* the occurrence of seizures and significant neuron loss,  
525 and were probably induced by dysfunctional glutamate-ammonia handling as the only  
526 known reaction catalyzed by Glul is the production of glutamine; a process which also  
527 results in inactivation of glutamate and detoxification of ammonia (Eid *et al.*, 2016). Here  
528 we demonstrated that deletion of Glul causes a major reduction in brain tissue levels of  
529 glutamine, glutamate and GABA. The reductions in glutamate and GABA probably reflect  
530 decreases in the neuronal transmitter pool as most tissue glutamate and GABA is in  
531 neurons (Danbolt, 2001). When glutamate cannot be amidated to glutamine, due to lack of  
532 Glul, glutamate is likely degraded via the glial tricarboxylic acid cycle rather than being  
533 transferred back to neurons as glutamine. Because glutamine is a precursor for the  
534 synthesis of neuronal glutamate and GABA, the lack of glutamine in the cKO cortex  
535 probably explains the low levels of the neurotransmitters. However, it is important to note  
536 that neurons may be able to synthesize glutamate *de novo* (Hassel and Bråthe, 2000) and  
537 that glutamate transporters in axon-terminals represent a mechanism for direct recycling  
538 independent of Glul (Danbolt *et al.*, 2016b; Zhou *et al.*, 2018). This may explain why *in*

539 *vitro* electrophysiological recordings show that axon-terminals can maintain basal  
540 glutamatergic neurotransmission during low extracellular glutamine conditions, whereas  
541 glutamine was only required for sustained high-frequency firing (Tani *et al.*, 2014). A  
542 reduction in total tissue glutamate does not necessarily indicate decreased extracellular  
543 glutamate. The episodes of wild-running and the occurrence of seizures in the Glul cKO  
544 mice are, however, suggestive of hyperexcitability, which may indicate increased  
545 extracellular glutamate. In support, these cKO mice have reductions in expression of  
546 glutamate transporters (EAAT1 and EAAT2), but these were moderate. Other factors that  
547 may contribute to increased excitability comprise reduced GABA levels and reductions in  
548 the GRIN2A glutamate receptor subunit. In addition, a conceptually distinct pathway of the  
549 control of cerebral blood flow mediated by glutamate transporters has been suggested,  
550 though it is unclear at the moment whether it is a direct or indirect effect (Petzold *et al.*,  
551 2008; Schummers *et al.*, 2008). Further, the brain has no urea cycle, and detoxification of  
552 ammonia by Glul is thereby the only significant mechanism apart from removal via blood.  
553 Consequently, Glul deficiency probably raises ammonia levels. The similarity between the  
554 ammonium ion and the potassium ion implies that ammonium ions can impair potassium  
555 buffering by interfering with several transporter proteins and subsequently weaken  
556 neuronal inhibition (Rangroo Thrane *et al.*, 2013). A raised  $[K^+]$  could affect the function of  
557 smooth muscle via inward rectifier  $K^+$  channels and dilates the vessels (Knot *et al.*, 1996).  
558 In conclusion, there are several factors that are likely to increase excitability, but we do not  
559 at this stage know their relative importance.

560       Even though the Glul cKO mice replicate several features of human TLE, there are  
561 notable differences. First, the mice are deficient in Glul in large portions of the cerebral  
562 cortex from early embryonic life, whereas patients with MTLE exhibit focal losses of Glul in  
563 the hippocampus and amygdala (Eid *et al.*, 2004; van der Hel *et al.*, 2005). Moreover, the  
564 Glul loss in human MTLE is probably not present during embryogenesis, but likely occurs

565 secondary to another insult, later in life. Despite these differences, we have clearly  
566 demonstrated that loss of Glul in the cerebral cortex leads to epilepsy and progressive  
567 neurodegeneration, which are key features of human MTLE. We have also shown that loss  
568 of astrocytic Glul leads to significant changes in cerebrovascular physiology, suggesting  
569 new and important roles of Glul in neurovascular biology.

570

## 571 **5. Conclusions**

572 In summary, Glul deficiency does not immediately lead to seizures via a classical  
573 excitotoxic syndrome, but rather triggers a prolonged pathological process involving early  
574 glial and cerebrovascular changes before progressive neuron loss become apparent.

575

## 576 **Acknowledgements**

577 We are grateful to the staff at the animal facility at The Norwegian Governmental Institute  
578 of Public Health for assisting with animal husbandry. This study was supported by the  
579 Norwegian Research Council (Grant no. 240844 to NCD), Novo Nordisk Fonden (Grant no.  
580 NNF14OC0010959 and NNF15OC0016528 to NCD), University of Oslo (SERTA to NCD;  
581 UNIFOR-FRIMED to NCD; PhD fellowship to HQX), and the National Institutes of Health  
582 (NIH, Grants number NS070824 to TE, RD and SEG; and MH067528 and NS052519 to  
583 FH). This work was also made possible by a grant from the National Center for Advancing  
584 Translational Sciences (NCATS; UL1 TR000142), a component of the NIH and the NIH  
585 Roadmap for Medical Research.

586

## 587 **Author contribution statement**

588 YZ and NCD designed the research; YZ managed the mouse colony, performed  
589 histological staining, immunocytochemistry, immunoblots and behavioral testing; RD and  
590 SEG performed the video-EEG recordings; MP performed the brain imaging; HQX carried



591 out histological staining and analyzed open field behavioral videos; BH quantified amino  
592 acids; YSP generated the Glul-flox mice; YZ, TE and NCD wrote the manuscript. All  
593 authors approved the final manuscript.

594

#### 595 **Conflict of interest**

596 The authors declare no competing financial interests.

597

#### 598 **References**

599 Attwell, D., Buchan, A.M., Charpak, S., Lauritzen, M., Macvicar, B.A., Newman, E.A.,  
600 2010. Glial and neuronal control of brain blood flow. *Nature* 468, 232-243.

601

602 Bernard-Helary, K., Ardourel, M.-Y., Hevor, T., Cloix, J.-F., 2002. In vivo and in vitro  
603 glycolytic effects of methionine sulfoximine are different in two inbred strains of mice.  
604 *Brain Res* 929, 147-155.

605

606 Blumenfeld, H., Varghese, G.I., Purcaro, M.J., Motelow, J.E., Enev, M., McNally, K.A.,  
607 Levin, A.R., Hirsch, L.J., Tikofsky, R., Zubal, I.G., Paige, A.L., Spencer, S.S., 2009.  
608 Cortical and subcortical networks in human secondarily generalized tonic-clonic seizures.  
609 *Brain* 132, 999-1012.

610

611 Coulter, D.A., Eid, T., 2012. Astrocytic regulation of glutamate homeostasis in epilepsy.  
612 *Glia* 60, 1215-1226.

613

614 Dahlberg, D., Ivanovic, J., Hassel, B., 2014. High extracellular concentration of excitatory  
615 amino acids glutamate and aspartate in human brain abscess. *Neurochem Int* 69, 41-47.

616

617 Danbolt, N.C., 2001. Glutamate uptake. *Prog Neurobiol* 65, 1-105.

618

619 Danbolt, N.C., Furness, D.N., Zhou, Y., 2016b. Neuronal vs glial glutamate uptake:  
620 Resolving the conundrum. *Neurochem Int* 98, 29-45.

621

622 Danbolt, N.C., Lehre, K.P., Dehnes, Y., Chaudhry, F.A., Levy, L.M., 1998. Localization of  
623 transporters using transporter-specific antibodies. *Methods Enzymol* 296, 388-407.

624

625 Danbolt, N.C., Zhou, Y., Furness, D.N., Holmseth, S., 2016a. Strategies for  
626 immunohistochemical protein localization using antibodies: What did we learn from  
627 neurotransmitter transporters in glial cells and neurons. *Glia* 64, 2045-2064.

628

629 Eid, T., Ghosh, A., Wang, Y., Beckstrom, H., Zaveri, H.P., Lee, T.-S.W., Lai, J.C.,  
630 Malthankar-Phatak, G.H., de Lanerolle, N.C., 2008. Recurrent seizures and brain  
631 pathology after inhibition of glutamine synthetase in the hippocampus in rats. *Brain* 131,  
632 2061-2070.

633

634 Eid, T., Gruenbaum, S.E., Dhaher, R., Lee, T.-S.W., Zhou, Y., Danbolt, N.C., 2016. The  
635 Glutamate-Glutamine Cycle in Epilepsy. In: *The Glutamate/GABA-Glutamine Cycle -*  
636 *Amino Acid Neurotransmitter Homeostasis* . Schousboe A and Sonnewald U, eds.  
637 Springer International Publishing. Switzerland.

638

639 Eid, T., Thomas, M.J., Spencer, D.D., Rundenpran, E., Lai, J.C.K., Malthankar, G.V., Kim,  
640 J.H., Danbolt, N.C., Ottersen, O.P., Delanerolle, N.C., 2004. Loss of glutamine synthetase  
641 in the human epileptogenic hippocampus: possible mechanism for raised extracellular  
642 glutamate in mesial temporal lobe epilepsy. *Lancet* 363, 28-37.

643

644 Eyo, U.B., Murugan, M., Wu, L.-J., 2017. Microglia-Neuron Communication in Epilepsy.  
645 *Glia* 65, 5-18.

646

647 Ferguson, R.E., Carroll, H.P., Harris, A., Maher, E.R., Selby, P.J., Banks, R.E., 2005.  
648 Housekeeping proteins: a preliminary study illustrating some limitations as useful  
649 references in protein expression studies. *Proteomics* 5, 566-571.

650

651 Gorski, J.A., Talley, T., Qiu, M., Puellas, L., Rubenstein, J.L., Jones, K.R., 2002. Cortical  
652 excitatory neurons and glia, but not GABAergic neurons, are produced in the Emx1-  
653 expressing lineage. *J Neurosci* 22, 6309-6314.

654

655 Haberle, J., Shahbeck, N., Ibrahim, K., Schmitt, B., Scheer, I., O'Gorman, R., Chaudhry,  
656 F.A., Ben-Omran, T., 2012. Glutamine supplementation in a child with inherited GS  
657 deficiency improves the clinical status and partially corrects the peripheral and central  
658 amino acid imbalance. *Orphanet J Rare Dis* 7, 48.

659

660 Hassel, B., Bråthe, A., 2000. Neuronal pyruvate carboxylation supports formation of  
661 transmitter glutamate. *J Neurosci* 20, 1342-1347.

662

663 He, Y., Hakvoort, T.B., Vermeulen, J.L., Labruyere, W.T., De Waart, D.R., Van Der Hel,  
664 W.S., Ruijter, J.M., Uylings, H.B., Lamers, W.H., 2010. Glutamine synthetase deficiency in  
665 murine astrocytes results in neonatal death. *Glia* 58, 741-754.

666

667 He, Y., Hakvoort, T.B., Vermeulen, J.L., Lamers, W.H., Van Roon, M.A., 2007. Glutamine  
668 synthetase is essential in early mouse embryogenesis. *Dev Dyn* 236, 1865-1875.

669

670 Holmseth, S., Dehnes, Y., Huang, Y.H., Follin-Arbelet, V.V., Grutle, N.J., Mylonakou, M.N.,  
671 Plachez, C., Zhou, Y., Furness, D.N., Bergles, D.E., Lehre, K.P., Danbolt, N.C., 2012b.

672 The density of EAAC1 (EAAT3) glutamate transporters expressed by neurons in the  
673 mammalian CNS. *J Neurosci* 32, 6000-6013.

674

675 Holmseth, S., Scott, H.A., Real, K., Lehre, K.P., Leergaard, T.B., Bjaalie, J.G., Danbolt,  
676 N.C., 2009. The concentrations and distributions of three C-terminal variants of the GLT1  
677 (EAAT2; slc1a2) glutamate transporter protein in rat brain tissue suggest differential  
678 regulation. *Neuroscience* 162, 1055-1071.

679

680 Holmseth, S., Zhou, Y., Follin-Arbelet, V.V., Lehre, K.P., Bergles, D.E., Danbolt, N.C.,  
681 2012a. Specificity controls for immunocytochemistry: the antigen pre-adsorption test can  
682 lead to inaccurate assessment of antibody specificity. *J Histochem Cytochem* 60, 174-187.

683

684 Kam, K., Nicoll, R., 2007. Excitatory synaptic transmission persists independently of the  
685 glutamate-glutamine cycle. *J Neurosci* 27, 9192-9200.

686

687 Knot, H.J., Zimmermann, P.A., Nelson, M.T., 1996. Extracellular K(+)-induced  
688 hyperpolarizations and dilatations of rat coronary and cerebral arteries involve inward  
689 rectifier K(+) channels. *J Physiol* 492 (Pt 2), 419-430.

690

691 Laemmli, U.K., 1970. Cleavage of structural proteins during the assembly of the head of  
692 bacteriophage T4. *Nature* 227, 680-685.

693

694 Lee, E.C., Yu, D., Martinez de Velasco, J., Tessarollo, L., Swing, D.A., Court, D.L.,

695 Jenkins, N.A., Copeland, N.G., 2001. A highly efficient Escherichia coli-based  
696 chromosome engineering system adapted for recombinogenic targeting and subcloning of  
697 BAC DNA. *Genomics* 73, 56-65.

698

699 Lehre, K.P., Levy, L.M., Ottersen, O.P., Storm-Mathisen, J., Danbolt, N.C., 1995.  
700 Differential expression of two glial glutamate transporters in the rat brain: quantitative and  
701 immunocytochemical observations. *J Neurosci* 15, 1835-1853.

702

703 Li, Y., Zhou, Y., Danbolt, N.C., 2012. The rates of postmortem proteolysis of glutamate  
704 transporters differ dramatically between cells and between transporter subtypes. *J*  
705 *Histochem Cytochem* 60, 811-821.

706

707 Lowry, O.H., 1953. The quantitative histochemistry of the brain. *J Histochem Cytochem* 1,  
708 420-428.

709

710 Lowry, O.H., Roberts, N.R., Leiner, K.Y., Wu, M.L., Farr, A.L., Albers, R.W., 1954. The  
711 quantitative histochemistry of brain, III. ammon's horn. *J Biol Chem* 207, 39-49.

712

713 Lowry, O.H., Rosebrough, N.J., Farr, A.L., Randall, R.J., 1951. Protein measurement with  
714 the Folin phenol reagent. *J Biol Chem* 193, 265-275.

715

716 Martinez-Hernandez, A., Bell, K.P., Norenberg, M.D., 1977. Glutamine synthetase: glial  
717 localization in brain. *Science* 195, 1356-1358.

718

719 McLin, J.P., Steward, O., 2006. Comparison of seizure phenotype and neurodegeneration  
720 induced by systemic kainic acid in inbred, outbred, and hybrid mouse strains. *Eur J*

721 Neurosci 24, 2191-2202.

722

723 Ortinski, P.I., Dong, J., Mungenast, A., Yue, C., Takano, H., Watson, D.J., Haydon, P.G.,  
724 Coulter, D.A., 2010. Selective induction of astrocytic gliosis generates deficits in neuronal  
725 inhibition. Nat Neurosci 13, 584-591.

726

727 Petzold, G.C., Albeanu, D.F., Sato, T.F., Murthy, V.N., 2008. Coupling of neural activity to  
728 blood flow in olfactory glomeruli is mediated by astrocytic pathways. Neuron 58, 897-910.

729

730 Racine, R.J., Burnham, W.M., Gartner, J.G., Levitan, D., 1973. Rates of motor seizure  
731 development in rats subjected to electrical brain stimulation: strain and inter-stimulation  
732 interval effects. Electroencephalogr Clin Neurophysiol 35, 553-556.

733

734 Rangroo Thrane, V., Thrane, A.S., Wang, F., Cotrina, M.L., Smith, N.A., Chen, M., Xu, Q.,  
735 Kang, N., Fujita, T., Nagelhus, E.A., Nedergaard, M., 2013. Ammonia triggers neuronal  
736 disinhibition and seizures by impairing astrocyte potassium buffering. Nat Med 19, 1643-  
737 1648.

738

739 Robel, S., Buckingham, S.C., Boni, J.L., Campbell, S.L., Danbolt, N.C., Riedemann, T.,  
740 Sutor, B., Sontheimer, H., 2015. Reactive astrogliosis causes the development of  
741 spontaneous seizures. J Neurosci 35, 3330-3345.

742

743 Robel, S., Sontheimer, H., 2016. Glia as drivers of abnormal neuronal activity. Nat  
744 Neurosci 19, 28-33.

745

746 Schummers, J., Yu, H., Sur, M., 2008. Tuned responses of astrocytes and their influence

747 on hemodynamic signals in the visual cortex. *Science* 320, 1638-1643.

748

749 Shaw, C.A., Bains, J.S., 2002. Synergistic versus antagonistic actions of glutamate and  
750 glutathione: the role of excitotoxicity and oxidative stress in neuronal disease. *Cell Mol Biol*  
751 (Noisy-le-grand) 48, 127-136.

752

753 Soriano, P., 1997. The PDGF alpha receptor is required for neural crest cell development  
754 and for normal patterning of the somites. *Development* 124, 2691-2700.

755

756 Spodenkiewicz, M., Diez-Fernandez, C., Rufenacht, V., Gemperle-Britschgi, C., Haberle,  
757 J., 2016. Minireview on Glutamine Synthetase Deficiency, an Ultra-Rare Inborn Error of  
758 Amino Acid Biosynthesis. *Biology (Basel)* 5, 40.

759

760 Tanaka, K., Watase, K., Manabe, T., Yamada, K., Watanabe, M., Takahashi, K., Iwama,  
761 H., Nishikawa, T., Ichihara, N., Kikuchi, T., Okuyama, S., Kawashima, N., Hori, S.,  
762 Takimoto, M., Wada, K., 1997. Epilepsy and exacerbation of brain injury in mice lacking  
763 the glutamate transporter GLT-1. *Science* 276, 1699-1702.

764

765 Tani, H., Dulla, C.G., Farzampour, Z., Taylor-Weiner, A., Huguenard, J.R., Reimer, R.J.,  
766 2014. A local glutamate-glutamine cycle sustains synaptic excitatory transmitter release.  
767 *Neuron* 81, 888-900.

768

769 van der Hel, W.S., Notenboom, R.G., Bos, I.W., van Rijen, P.C., van Veelen, C.W., de  
770 Graan, P.N., 2005. Reduced glutamine synthetase in hippocampal areas with neuron loss  
771 in temporal lobe epilepsy. *Neurology* 64, 326-333.

772

773 Verkhatsky, A., Sofroniew, M.V., Messing, A., deLanerolle, N.C., Rempe, D., Rodriguez,  
774 J.J., Nedergaard, M., 2012. Neurological diseases as primary gliopathies: a reassessment  
775 of neurocentrism. *ASN Neuro* 44, art:e00082.

776

777 Wolf, S.A., Boddeke, H.W., Kettenmann, H., 2017. Microglia in Physiology and Disease.  
778 *Annu Rev Physiol* 79, 619-643.

779

780 Wurst, W., Joyner, A.L., 1999. Production of targeted embryonic stem cell clones. In: *Gene*  
781 *Targeting: A Practical Approach*. Joyner AL, eds. Oxford University Press. New York.

782

783 Zhou, Y., Hassel, B., Eid, T., Danbolt, N.C., 2018. Axon-terminals expressing EAAT2  
784 (GLT-1; Slc1a2) are common in the forebrain and not limited to the hippocampus.  
785 *Neurochem Int*, IN PRESS.

786

787 Zhou, Y., Holmseth, S., Hua, R., Lehre, A.C., Olofsson, A.M., Poblete-Naredo, I.,  
788 Kempson, S.A., Danbolt, N.C., 2012. The betaine-GABA transporter (BGT1, slc6a12) is  
789 predominantly expressed in the liver and at lower levels in the kidneys and at the brain  
790 surface. *Am J Physiol Renal Physiol* 302, F316-328.

791

792 Zhou, Y., Waanders, L.F., Holmseth, S., Guo, C., Berger, U.V., Li, Y., Lehre, A.-C., Lehre,  
793 K.P., Danbolt, N.C., 2014. Proteome analysis and conditional deletion of the EAAT2  
794 glutamate transporter provide evidence against a role of EAAT2 in pancreatic insulin  
795 secretion in mice. *J Biol Chem* 289, 1329-1344.

796

797



798 **Figure legends**

799

800 **Fig. 1.** Selective deletion of the Glul gene in the cerebral cortex was achieved by crossing  
801 Emx1-Cre mice with Glul-flox mice. **(A)** Construction of Glul flox mice (see Methods for  
802 details). **(B)** The resulting Glul conditional knockout mice (cKO) lacked Glul protein in the  
803 neocortex and the hippocampus. Sections through different parts of brains from cKO and  
804 wild-type (WT) mice were labeled with antibodies to Glul. Note that there is hardly any  
805 staining in the cerebral cortex (\*) of the cKO mice. And as the Emx1-Cre driver is not  
806 active in the cerebellum (cb), Glul expression is preserved. Scale bar 1 mm. **(C)**  
807 Immunoblots confirmed that Glul labeling was virtually absent in the hippocampus and  
808 neocortex of the cKO mice. Identical blots were prepared from fresh brain tissue from the  
809 hippocampus (hip), neocortex (neo), cerebellum (cb) and rest of the brain (rb) from cKO  
810 and WT mice, and probed with antibodies to Glul or EAAT3 as indicated. **(D)** Mortality of  
811 the cKOs during 16-week-observation period (n = 97). Note that the mortality was highest  
812 between 4 weeks and 9 weeks with few deaths before and after.

813 **Fig.2.** Glul conditional knockout (cKO) mice exhibited altered locomotive activities when  
814 subjected to the 15-min open-field test. A total of 15 pairs of WT and cKO mice (21 - 103  
815 days old) were tested (10 pairs of males and 5 pairs of females). **(A)** Most of the cKO mice  
816 (cKO1; 9 pairs) were clearly hypoactive during the entire test period. **(B)** The remainder  
817 (cKO2; 6 pairs) had one or more sudden bursts of activity during the test period. The  
818 number of total crossings of all groups of cKO1 and cKO2 were represented in Panel **(C)**.  
819 **(D)** The cKO mice were less active vertically (lower number of rearings), **(E)** they had  
820 fewer entries to the center, **(F)** but spent comparable time in the center. **(G)** The cKO also  
821 produced a lower number of feces during the test session. \*\*p<0.01

822

823 **Fig. 3. (A)** The bars indicate the average number of seizures from the animals in c after  
824 exclusion of the 7 cKO that died during recordings. No seizures were observed in the  
825 wildtype (WT) or heterozygous Glul knockout (Het) mice, whereas the cKO mice had an  
826 average of  $2.71 \pm 1.13$  seizures during the 2-week period ( $p = 0.002$ ). Twelve of 19 (63.2%)  
827 seizures were severe (Racine Grade 4-5). **(B)** Representative EEG tracing of a WT mouse  
828 and representative EEG tracing of a cKO mouse are shown. The arrow indicates the start  
829 of the seizure. The severity of the seizure was not apparent by EEG, and examination of  
830 the concurrent video record was necessary for severity staging. **(C)** Daily seizure counts  
831 and severity assessments over a 14-day recording period. Wildtype (WT;  $n = 11$ : 6 males,  
832 5 females), heterozygous Glul knockout (Het;  $n = 9$ : 7 males, 2 females), and homozygous  
833 Glul knockout (cKO;  $n = 14$ : 9 males, 5 females) mice were monitored by continuous  
834 video-intracranial EEG analysis for two-weeks. The number of seizures per day is provided.  
835 Mild (Racine Grade 1-3) and severe (Racine Grade 4-5) seizures are indicated by blue  
836 and red numbers respectively. Seven of the 14 cKO animals died at different time points  
837 during the recording (indicated by dark gray shading). These animals are excluded from  
838 the plots in **A**. Abbreviations: F, female; M, male.

839

840 **Fig. 4.** Mice lacking Glul in the cerebral cortex had progressive neurodegeneration. Nissl  
841 **(A)** and NeuroSilver **(B)** staining of hippocampus of WT and cKO mice showed massive  
842 neuronal degenerations (arrows) in CA1, in CA3, in part of the granule cell layer and in the  
843 hilus of the dentate gyrus (DG) at 11 weeks of age, but not at 4.5 weeks. **(C)** Nissl and **(D)**  
844 Neurosilver staining of motor cortex of Glul wildtype and conditional knockouts (cKO)  
845 showing massive neuronal degenerations in upper layer of cortex at 9 weeks of age. No  
846 neuron degenerations were seen at 4-5 weeks of age. **(E)** Selective degeneration in some  
847 areas of cortex indicated by red arrows. Scale bar: 50  $\mu\text{m}$  **(A-D)**; 1 mm **(E)**.

848 **Fig. 5.** Lack of cortical Glul leads to astrogliosis preceding neurodegeneration. **(A)**  
849 Sections from the neocortex of WT and cKO mice (littermates processed in parallel; ages  
850 as indicated) were probed with antibodies to GFAP (green; labels astrocytes). Astrogliosis,  
851 as indicated by increased GFAP expression, was evident in the neocortex and  
852 hippocampus CA1 of 4 weeks old cKO mice. In contrast, thalamus in the cKO (where  
853 Emx1-Cre is not active) showed normal expression of GFAP at both age groups. Scale bar  
854 50  $\mu\text{m}$ . **(B)** GFAP expression increases with age being statistically significantly increased  
855 at four weeks of age. The expression levels were quantified by immunoblotting of  
856 hippocampi from wild-type (WT) and Glul cortical knockout (cKO) mice: five pairs of WT  
857 and cKO littermates in each age group: 2 weeks of age n = 5 pairs: 3 pairs of males, 2  
858 pairs of females; 4 weeks of age n = 5 pairs: 2 pairs of males, 3 pairs of females; >12  
859 weeks of age n = 5 pairs: 4 pairs of males, 1 pair of females; \* $p < 0.05$ , \*\* $p < 0.01$ .

860  
861 **Fig. 6.** Glul knockout mice (cKO) had altered cerebral blood vessels with reduced ability to  
862 react to increases in CO<sub>2</sub> levels. **(A)** There was increased GFAP labeling (green) in  
863 astroglial processes in 3 weeks old Glul cKO mice. The images from wildtype (WT) and  
864 cKO mice represent montages of three overlapping images acquired from the motor cortex.  
865 Scale bar 100  $\mu\text{m}$ . **(B)** Z-stack image (total thickness 9.5  $\mu\text{m}$ ) acquired from motor cortex  
866 (layer VI) of the same cKO section as in **A**. Note increased GFAP labeling in astroglial  
867 processes surrounding blood vessels (red, GLUT1). Scale bar 100  $\mu\text{m}$ . **(C)** Nissl staining  
868 shows changed vascular structures in the motor cortex and hippocampus CA1 of 9 weeks  
869 old cKO mice compared to WT littermates (processed in parallel). Scale bar 50  $\mu\text{m}$ . **(D)**  
870 Impaired cerebrovascular reactivity in (as indicated) 4 and 12 - 15 weeks old cKO  
871 mice. Voxel-level maps of cerebrovascular reactivity (CVR), as defined by the relative  
872 increase of signal during CO<sub>2</sub> challenge, averaged across each age/group. Maps are  
873 projected on two coronal slices of a structural mouse atlas. Region of interest-averaged

874 CVR amplitudes are shown on bar graphs (bottom); cKO mice have impaired CVR  
875 response in the dorsal hippocampus at 12 weeks, and in the cortex at both time-points.  
876 Subcortical areas like the basal forebrain are unaffected in cKO animals. The most cranial  
877 slices (the left images on each sub-figure) are +1.2 mm from bregma, while the caudal  
878 slices (the right images on each sub-figure) are -0.6 mm from bregma. \* $p < 0.05$ ; \*\*  $p <$   
879 0.01.

880

881 **Fig. 7.** Several of the components of the glutamatergic signaling system were altered in  
882 Glul cortical knockout (cKO) mice. **(A)** Taqman RT-PCR revealed statistically significant  
883 reductions in the expression of glutamate transporter EAAT2 (\*\* $p < 0.01$ ) and of the  
884 glutamate receptor subunits GRIA1 (\*\* $p < 0.01$ ) and GRIN2A (\*\* $p < 0.01$ ) in the  
885 hippocampi of 5 weeks old cKO mice compared to their wild-type (WT) littermates ( $n = 4$   
886 pairs of male mice). In contrast, the expression of GRIN2C ( $p = 0.119$ ), GRM3 ( $p = 0.128$ )  
887 and EAAT1 ( $p = 0.606$ ) were not changed. The expression levels were normalized with  
888 that of GAPDH (control). **(B)** Immunoblots showed statistically significant (\* $p < 0.05$ ; \*\*  $p <$   
889 0.01) reduction in expression of glutamate transporter proteins in the hippocampus of  
890 young cKO mice compared to their WT littermates (2 weeks of age  $n = 5$  pairs: 3 pairs of  
891 males, 2 pairs of females; 4 weeks of age  $n = 5$  pairs: 2 pairs of males, 3 pairs of  
892 females; >12 weeks of age  $n = 5$  pairs: 4 pairs of males, 1 pair of females). Note that  
893 EAAT2 was the most affected subtype and that the strongest reduction was in the  
894 youngest mice. In contrast, the vesicular glutamate transporter 1, VGLUT1, was hardly  
895 reduced ( $n = 3$  pairs of WT and cKO mice).

896

897 Table 1. Total amino acids in the cerebral cortex (including hippocampus) from cortical  
 898 Glul knockouts and wildtype littermates

	Cortex		Cerebellum	
	WT (Cre <sup>-</sup> ; GS <sup>f/f</sup> )	cKO (Cre <sup>+</sup> ; GS <sup>f/f</sup> )	WT (Cre <sup>-</sup> ; GS <sup>f/f</sup> )	cKO (Cre <sup>+</sup> ; GS <sup>f/f</sup> )
<b>Asp</b>	2.86 ± 0.52	0.86 ± 0.19*	2.24 ± 0.36	2.38 ± 0.31
<b>Glu</b>	9.45 ± 1.76	4.82 ± 0.52*	8.17 ± 0.33	8.58 ± 0.59
<b>Gln</b>	4.39 ± 0.24	1.05 ± 0.25*	4.81 ± 0.30	4.90 ± 1.17
<b>Tau</b>	10.20 ± 2.87	12.43 ± 0.89	6.09 ± 0.13	7.46 ± 0.79
<b>Ala</b>	0.84 ± 0.16	0.93 ± 0.10	0.25 ± 0.17	0.30 ± 0.12
<b>GABA</b>	1.55 ± 0.48	0.82 ± 0.18*	1.08 ± 0.36	1.08 ± 0.03

899  
 900 Amino acid concentrations (nmol per mg wet weight of whole tissue) were determined by  
 901 means of HPLC in samples from three conditional Glul cortical knockouts (cKO) and two  
 902 wildtype littermates. The mice, all females, were about 8 weeks old. The cortex samples  
 903 comprised the entire neocortex and hippocampus. The numbers represent mean ± SD.

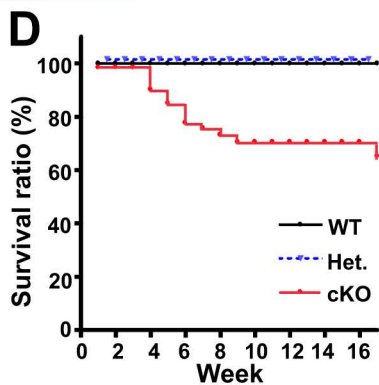
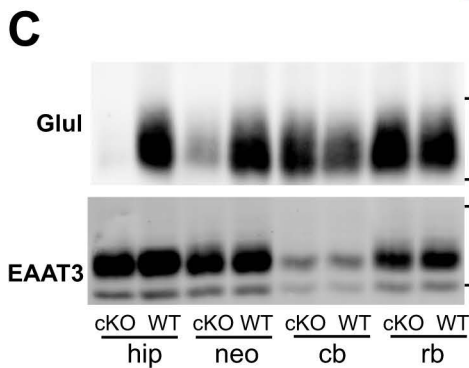
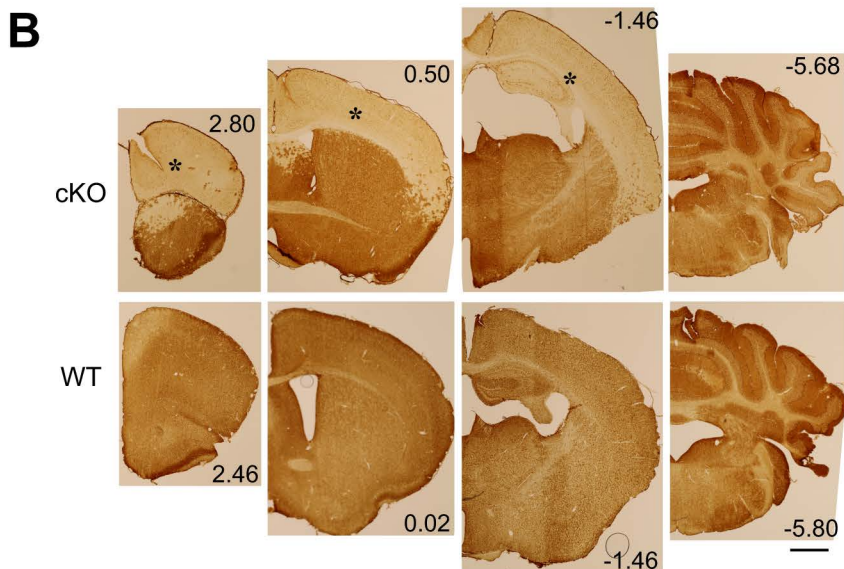
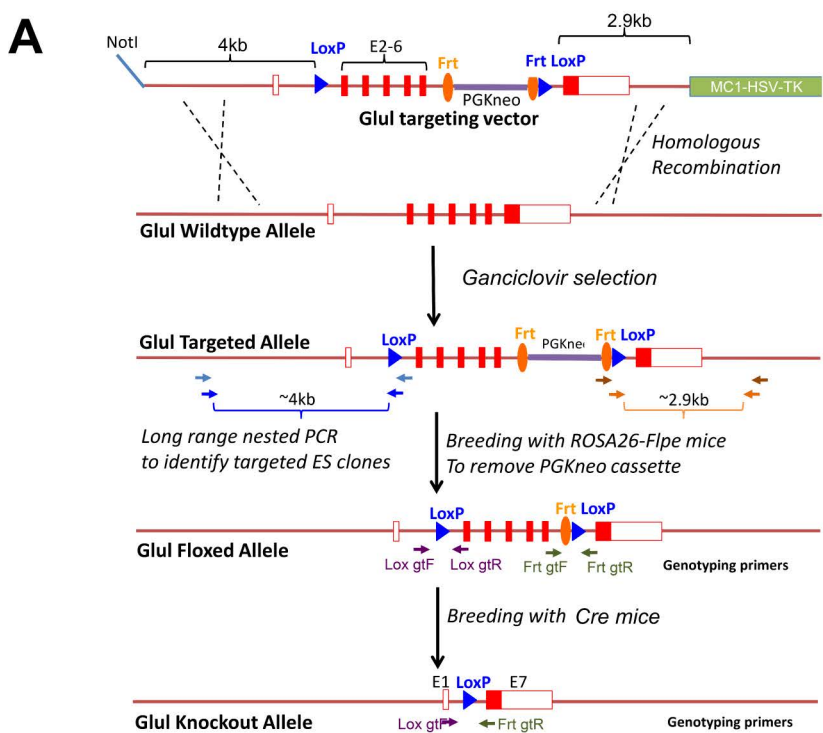


**Figure 1**

## Open-Field Test

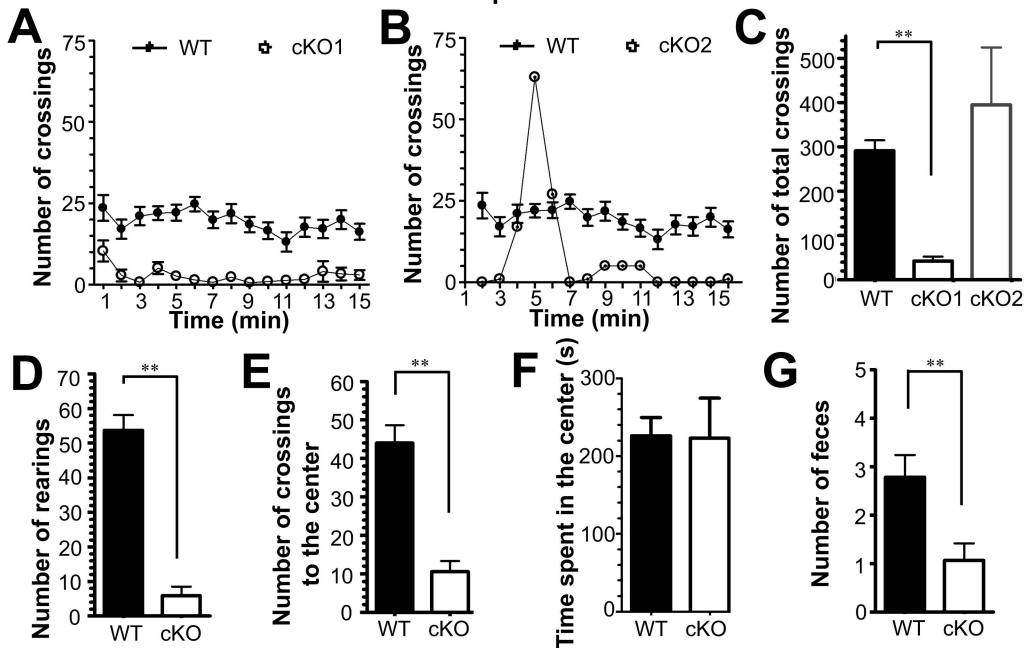
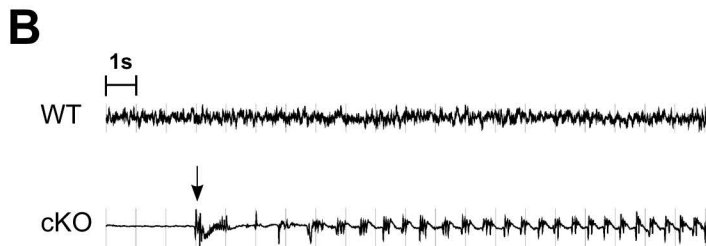
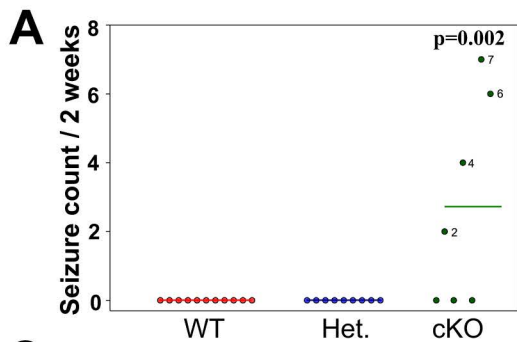


**Figure 2**



**C**

Mouse ID	Age (days)	Genotype	Sex	Days of EEG Analysis														Total Seizures
				1	2	3	4	5	6	7	8	9	10	11	12	13	14	
1.5M5	33	WT	M	0	0	0	0	0	0	0	0	0	0	0	0	0	0	0
4.3M3	38	WT	M	0	0	0	0	0	0	0	0	0	0	0	0	0	0	0
4.3M4	38	WT	M	0	0	0	0	0	0	0	0	0	0	0	0	0	0	0
4.3F1	38	WT	F	0	0	0	0	0	0	0	0	0	0	0	0	0	0	0
3.4M2	40	WT	M	0	0	0	0	0	0	0	0	0	0	0	0	0	0	0
3.4F3	40	WT	F	0	0	0	0	0	0	0	0	0	0	0	0	0	0	0
4.1F3	86	WT	F	0	0	0	0	0	0	0	0	0	0	0	0	0	0	0
4.6F1	152	WT	F	0	0	0	0	0	0	0	0	0	0	0	0	0	0	0
2.4F1	152	WT	F	0	0	0	0	0	0	0	0	0	0	0	0	0	0	0
1.4M2	166	WT	M	0	0	0	0	0	0	0	0	0	0	0	0	0	0	0
2.3M4	208	WT	M	0	0	0	0	0	0	0	0	0	0	0	0	0	0	0
3.4M3	40	Het	M	0	0	0	0	0	0	0	0	0	0	0	0	0	0	0
3.4F2	40	Het	F	0	0	0	0	0	0	0	0	0	0	0	0	0	0	0
8.3 M1	40	Het	M	0	0	0	0	0	0	0	0	0	0	0	0	0	0	0
9.2 M1	43	Het	M	0	0	0	0	0	0	0	0	0	0	0	0	0	0	0
9.2 M2	43	Het	M	0	0	0	0	0	0	0	0	0	0	0	0	0	0	0
9.2M3	43	Het	M	0	0	0	0	0	0	0	0	0	0	0	0	0	0	0
6.2M10	69	Het	M	0	0	0	0	0	0	0	0	0	0	0	0	0	0	0
9.3F2	93	Het	F	0	0	0	0	0	0	0	0	0	0	0	0	0	0	0
2.3M1	208	Het	M	0	0	0	0	0	0	0	0	0	0	0	0	0	0	0
1.5M1	33	cKO	M	0	0	0	0	0	0	0	0	0	0	0	0	0	0	0
1.5M3	33	cKO	M	0	0	0	0	0	0	0	1	0	0	1	0	0	0	0,2
3.4M1	38	cKO	M	0	0													0
8.3M4	38	cKO	M	0	0	0	0											0
11.4F2	61	cKO	F	0	0	0	0	0	0	0	0	0	0	0	0	0	0	0
11.4F6	61	cKO	F	0	0													0
8.5M1	69	cKO	M	0	0	0	0	0	0	0	0	0	1	1,1	1	0	0	3,1
8.5M6	69	cKO	M	0	0	0	0	0	0	0	0	0	0	0	0	0	0	0
6.2M2	69	cKO	M	2	1	10,5	4,2											16,8
6.2M6	69	cKO	M	0	0													0
6.2M7	69	cKO	M	2	0	43,7	41,3											84,12
6.2F3	69	cKO	F	0	0													0
4.1F2	86	cKO	F	3	0	0	0	1	0	0	0	0	1	1,1	0	0	0	4,3
2.4F2	152	cKO	F	0	0	0	0	4	0	0	0	0	0	1	0	1	0	0,6

**Figure 3**



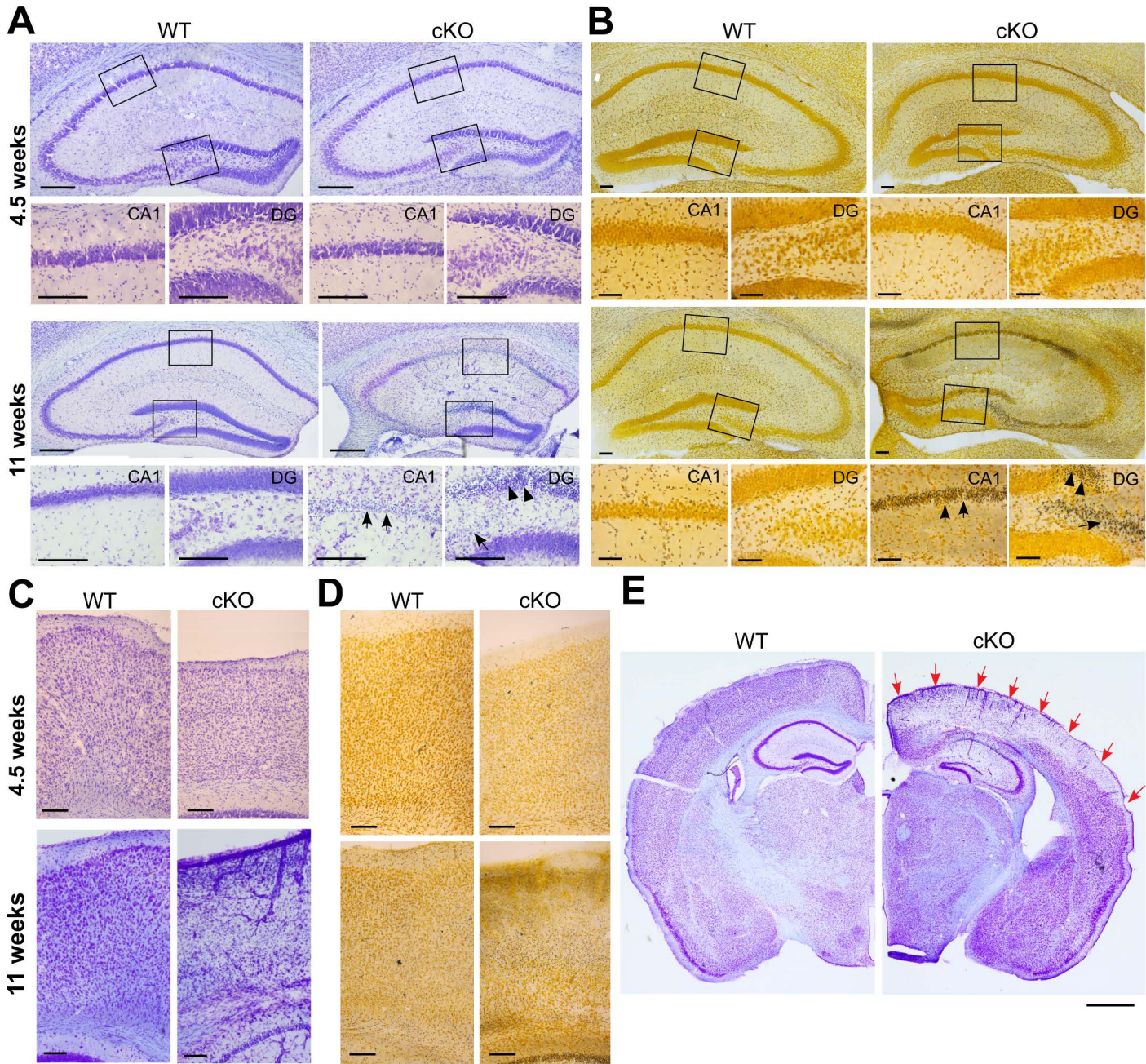


**Figure 4**

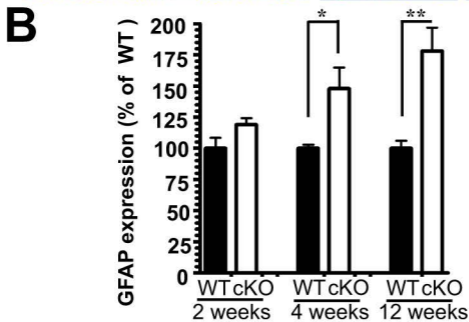
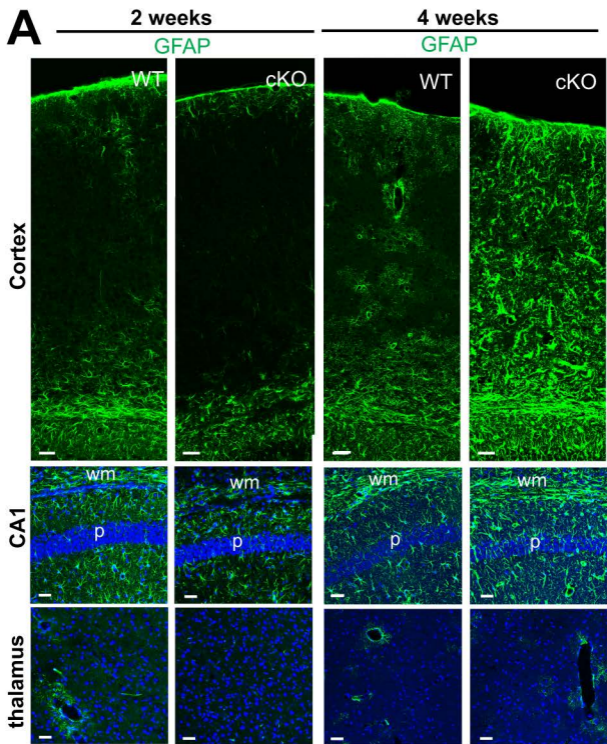


**Figure 5**

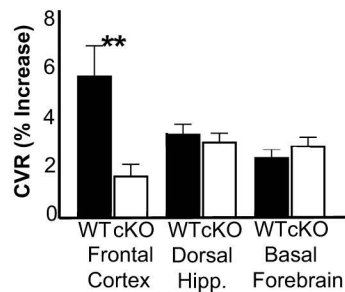
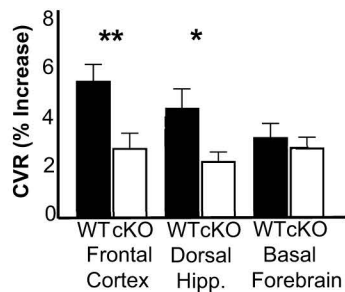
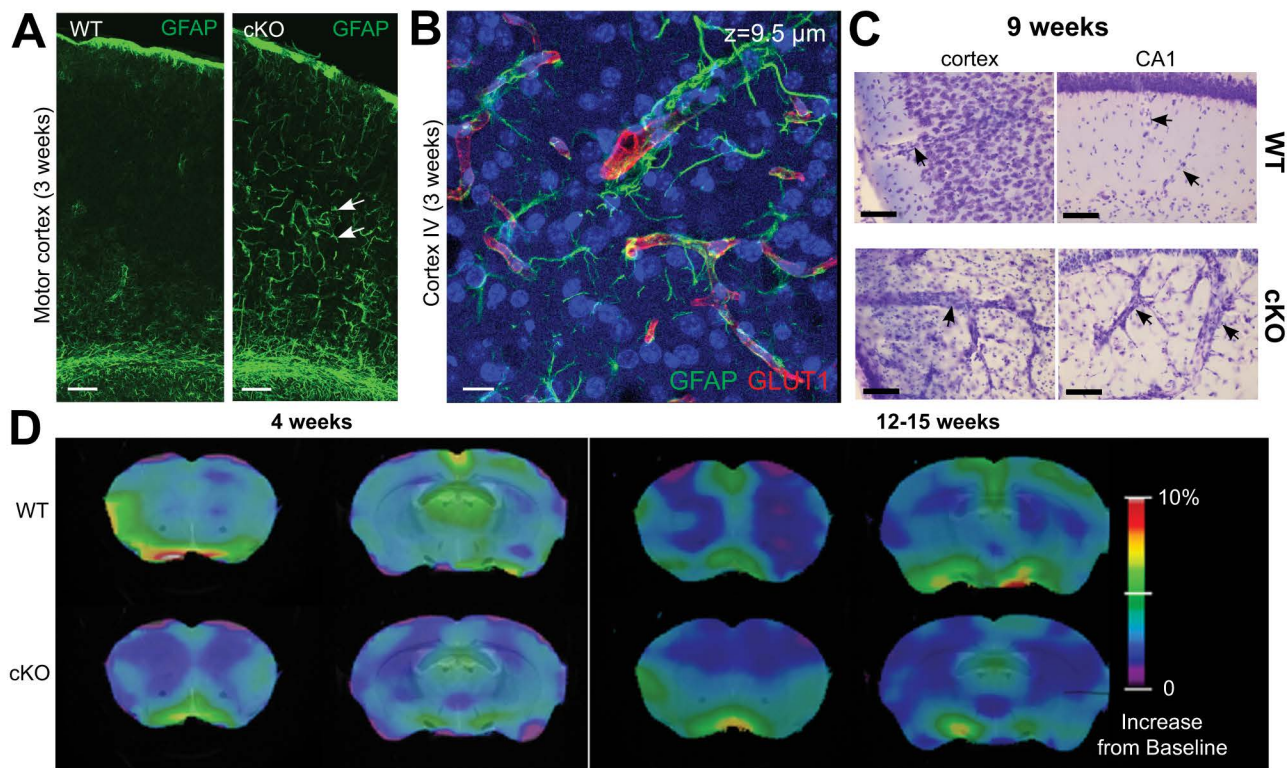


**Figure 6**

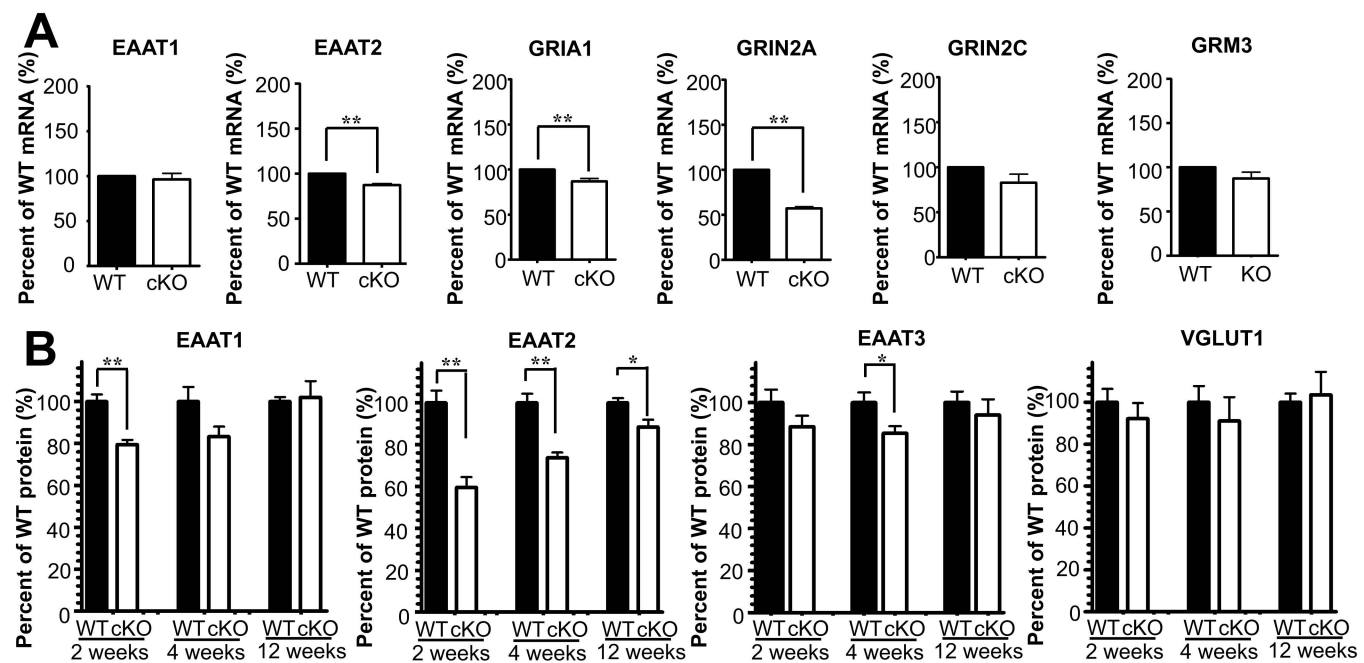


**Figure 7**